JACS
JOURNAL OF THE AMERICAN CHEMICAL SOCIETY
Article
pubs.acs.org/JACS

Coexistence of Magnetic Order and Ferroelectricity at 2D Nanosheet Interfaces

Bao-Wen Li,[†] Minoru Osada,[*,†] Yasuo Ebina,[†] Shigenori Ueda,[‡,§] and Takayoshi Sasaki[*,†]

[†]International Center for Materials Nanoarchitectonics (WPI-MANA), National Institute for Materials Science (NIMS), Tsukuba, Ibaraki 305-0044, Japan

[‡]Synchrotron X-ray Station at SPring-8, National Institute for Materials Science (NIMS), Sayo, Hyogo 679-5148, Japan

[§]Quantum Beam Unit, National Institute for Materials Science (NIMS), Tsukuba, Ibaraki 305-0047, Japan

Supporting Information

ABSTRACT: Multiferroic materials, in which the electronic polarization can be switched by a magnetic field and vice versa, are of fundamental importance for new electronic technologies. However, there exist very few single-phase materials that exhibit such cross-coupling properties at room temperature, and heterostructures with a strong magnetoelectric coupling have only been made with complex techniques. Here, we present a rational design for multiferroic materials by use of a layer-by-layer engineering of 2D nanosheets. Our approach to new multiferroic materials is the artificial construction of high-quality superlattices by interleaving ferromagnetic $Ti_{0.8}Co_{0.2}O_2$ nanosheets with dielectric perovskite-structured $Ca_2Nb_3O_{10}$ nanosheets. Such an artificial structuring allows us to engineer the interlayer coupling, and the ($Ti_{0.8}Co_{0.2}O_2/Ca_2Nb_3O_{10}/Ti_{0.8}Co_{0.2}O_2$) superlattices induce room-temperature ferroelectricity in the presence of the ferromagnetic order. Our technique provides a new route for tailoring artificial multiferroic materials in a highly controllable manner.

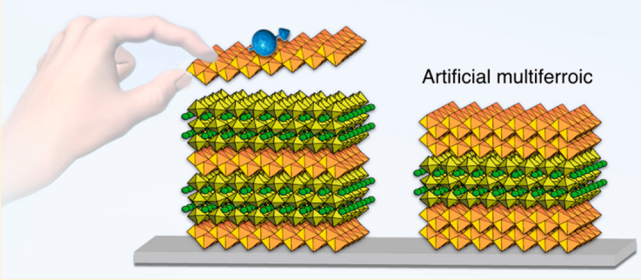

INTRODUCTION

Multiferroic materials, in which magnetism coexists with ferroelectricity, have attracted a great interest, and emerging physical properties and novel functionalities have inspired extensive research efforts.[1−5] A prominent feature of such multiferroic materials is the cross correlation phenomenon between the ferromagnetic and ferroelectric orders, the so-called magnetoelectric (ME) effect, which provides an additional order parameter for designing novel multifunctional devices. Although the ME effects at room temperature (RT) would be ideal for the practical use, there exist very few single-phase materials with the coexistence of ferromagnetism and ferroelectricity at RT.[6]

One approach to new multiferroic materials is to engineer an interlayer coupling at the interface between magnetic and ferroelectric systems. Recently, composite materials comprising ferromagnetic and ferroelectric layers were fabricated by state-of-the-art thin-film technologies involving molecular-beam epitaxy, and new classes of two-phase multiferroic materials such as granular materials, laminates, and epitaxial multilayers were developed, thereby opening a new era in this field.[1,4,7] In these approaches, researchers can draw from the large group of magnetic and ferroelectric materials and fabricate artificial multiferroics through the interface engineering between two ferroic orders. However, current techniques of such artificial systems require complex fabrication processes involving high-temperature annealing (>400 °C), causing a degradation of the interface properties. Also, because of the constraints of current film technologies, engineered ME behavior is still limited by the choice of materials and their coupling intensity.

Here, we demonstrate a new chemical design for artificial multiferroics using 2D oxide nanosheets as building blocks (Figure 1). This approach enables engineering of the interlayer coupling between the ferromagnetic and ferroelectric orders, as demonstrated by artificial superlattices composed of ferromagnetic $Ti_{0.8}Co_{0.2}O_2$ nanosheets and dielectric perovskite-structured $Ca_2Nb_3O_{10}$ nanosheets. ($Ti_{0.8}Co_{0.2}O_2/Ca_2Nb_3O_{10}/Ti_{0.8}Co_{0.2}O_2$) superlattices exhibit ME effects at RT, which can be modulated by tuning the interlayer coupling (i.e., the stacking sequence). Our study opens a pathway to create new artificial materials with tailored multiferroic properties.

RESULTS AND DISCUSSION

Hybrid Nanoarchitectures Formed by Ferromagnetic and Dielectric Nanosheets. Our chemical approach is based on artificial construction of ferromagnetic/ferroelectric heterostructures using the superlattice assembly of two different nanosheets (Figure 1). As the ferromagnetic component, we chose $Ti_{0.8}Co_{0.2}O_2$ (Figure 1a), an RT ferromagnetic nanosheet derived from the exfoliation of a layered titanate ($K_{0.8}Ti_{1.6}Co_{0.4}O_4$).[8,9] This nanosheet is a new type of 2D

Received: March 15, 2016
Published: June 13, 2016

 © 2016 American Chemical Society
DOI: 10.1021/jacs.6b02722
J. Am. Chem. Soc. 2016, 138, 7621−7625

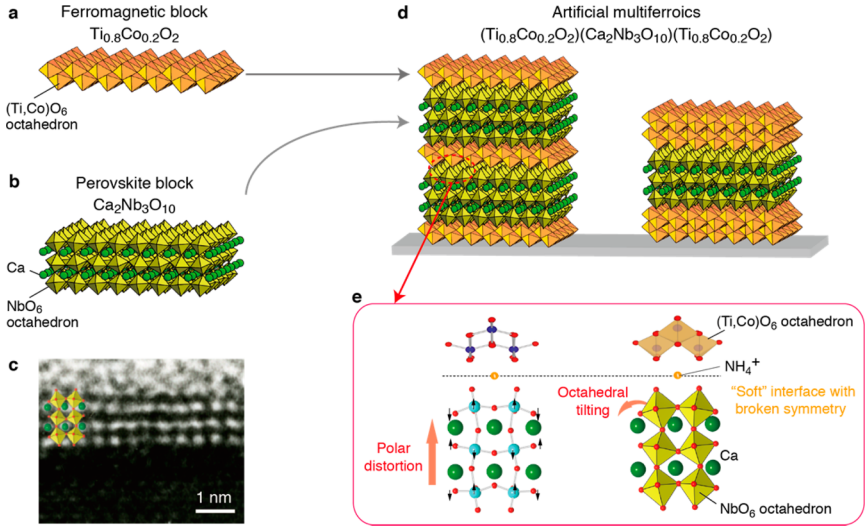

Figure 1. Tuning interlayer coupling in nanosheet architectures. (a and b) Structural models for nanosheets ($Ti_{0.8}Co_{0.2}O_2$ and $Ca_2Nb_3O_{10}$). (c) High-resolution TEM image of $Ca_2Nb_3O_{10}$ nanosheet. (d) Artificial multiferroic materials fabricated from nanosheet architectures. (e) Interface structure at the nanosheet architecture ($Ti_{0.8}Co_{0.2}O_2/Ca_2Nb_3O_{10}$).

ferromagnet with a magnetic moment of ~1 μ_B/Co and T_C of ~350 K. For a dielectric component, we used high-*k* dielectric perovskite, $Ca_2Nb_3O_{10}$, derived from a layered perovskite ($KCa_2Nb_3O_{10}$) by exfoliation (Figure 1b).[10,11] An important aspect is that $Ca_2Nb_3O_{10}$ nanosheet consists only of three NbO_6 octahedral nanoblocks with a large molecular polarizability. $Ca_2Nb_3O_{10}$ nanosheet can thus be regarded as an ideal base for high-*k* dielectrics and ferroelectrics with a critical thickness (Figure 1c). Using $Ca_2Nb_3O_{10}$ as a key building block, we fabricated layered perovskites sandwiched with ferromagnetic $Ti_{0.8}Co_{0.2}O_2$ (Figure 1d).

We utilized the Langmuir–Blodgett (LB) process for the fabrication of superlattice films.[12−14] The substrate such as atomically flat $SrRuO_3$ was placed vertically inside the LB trough. During the LB process, the packing density of the nanosheets could be controlled via the surface pressure of the air–water interface. The highly condensed phase appeared at the surface pressures at 10 mN m^{-1} ($Ti_{0.8}Co_{0.2}O_2$) and 15 mN m^{-1} ($Ca_2Nb_3O_{10}$), respectively, and the resulting monolayer films yielded 95% coverage with only occasional overlaps and gaps (Figure S1). Under the optimized surface pressure, the procedure for the LB depositions was repeated to synthesize a superlattice assembly. The resulting superlattice films were irradiated with UV white light from an Xe lamp (4 mW cm^{-2}) for 48 h in order to decompose the tetrabuthylammonium (TBA) hydroxide ions used in the exfoliation process. In conjunction with previous FT-IR data,[15] the UV-treated films can be analyzed on the basis of an inorganic multilayer assembly accommodating NH_4^+ ions (Figure 1e) as a consequence of the total photocatalytic removal of TBA ions.

Successful deposition of the superlattice films was confirmed by UV–visible absorption spectra. Figure 2a,b shows the variation of the absorption spectra in two different superlattices. From a comparison with the absorption data for the multilayer films (Figure S2), the absorption peaks at 275 and 232 nm are attributable to $Ti_{0.8}Co_{0.2}O_2$ and $Ca_2Nb_3O_{10}$ nanosheets, respectively, and each deposition cycle causes progressive enhancements for regular growth of $Ti_{0.8}Co_{0.2}O_2$ and $Ca_2Nb_3O_{10}$ nanosheet films with the designed sequences.

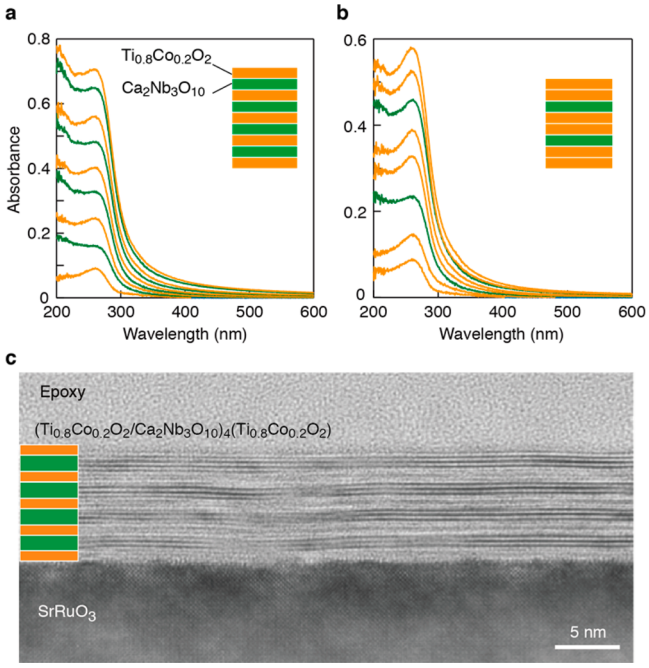

Figure 2. Superlattice engineering of 2D oxide nanosheets. Superlattice buildup process monitored by UV–visible spectroscopy: (a) $(Ti_{0.8}Co_{0.2}O_2/Ca_2Nb_3O_{10})_4/(Ti_{0.8}Co_{0.2}O_2)_1$, (b) $[(Ti_{0.8}Co_{0.2}O_2)_2/Ca_2Nb_3O_{10}]_2/(Ti_{0.8}Co_{0.2}O_2)_2$. (c) HRTEM image of $(Ti_{0.8}Co_{0.2}O_2/Ca_2Nb_3O_{10})_4/Ti_{0.8}Co_{0.2}O_2$ superlattice on $SrRuO_3$ substrate.

The superlattice films were also examined by X-ray diffraction (XRD) and high-resolution transmission electron microscopy (HRTEM). In $(Ti_{0.8}Co_{0.2}O_2/Ca_2Nb_3O_{10})_4/Ti_{0.8}Co_{0.2}O_2$ superlattice, the out-of-plane XRD data exhibited two Bragg peaks (at 6.1 and 10°) with *d* spacing values of 1.4 and 0.9 nm (Figure S3). The obtained value of d = 1.4 nm for the first peak is approximately half of the repeating unit of each $Ca_2Nb_3O_{10}$ and $Ti_{0.8}Co_{0.2}O_2$ nanosheet (d = 2.8 nm = 1.6 + 1.2 nm), and the reflection in the superlattice can be ascribed to the second-order line of the superlattice. Cross-sectional HRTEM (Figure 2c) provides direct structural information on the nanosheet superlattices. The TEM image of the

DOI: 10.1021/jacs.6b02722
J. Am. Chem. Soc. 2016, 138, 7621−7625

$(Ti_{0.8}Co_{0.2}O_2/Ca_2Nb_3O_{10})_4/Ti_{0.8}Co_{0.2}O_2$ superlattice revealed the homogeneous film architecture over the substrate surface, showing the superlattice structure composed of $Ti_{0.8}Co_{0.2}O_2$ and $Ca_2Nb_3O_{10}$ layers. The thicknesses of the constituent layers are approximately 1.0 and 1.6 nm, which agrees well with the crystallographic thicknesses of 0.75 nm for $Ti_{0.8}Co_{0.2}O_2$ and 1.45 nm for $Ca_2Nb_3O_{10}$ nanosheets. One more important aspect is the realization of high-quality, sharp heterointerfaces. In perovskite thin films, the formation of the interfacial dead layers is a longstanding problem, which causes the degradation of dielectric/ferroelectric properties. In our case, there was no detectable intermixing at the interface, suggesting the production of the perovskite superlattice without dead layers. We also note that superlattice films of a similar quality were achieved in different stacking sequences and with different substrates such as $SrTiO_3$:Nb or Si. In our approach, the exact control of interface engineering can be realized in the layer-by-layer assembled superlattices.

Magnetoelectric Effects in Nanosheet Architectures. We have investigated the ME properties of the nanosheet superlattices. We note that the structure of our artificial superlattice is analogous to that of Bi-layered perovskite ferroelectrics ($Bi_{4-x}La_xTi_3O_{12}$).[16] Even in a paraelectric ground of $Ca_2Nb_3O_{10}$ nanosheets (Figure S4), such an engineered interface with a broken symmetry can induce the ferroelectric order, offering the possibility of manipulating the electronic polarization by a magnetic field and vice versa. Also, considering the versatility of materials choice and their interface structures, we can create a new kind of layered perovskite multiferroics, in similar to Aurivillius compounds ($Bi_{m+1}Fe_{m-3}Ti_3O_{3m+3}$; m = 4−9).[17]

Figure 3 shows the dielectric/magnetic properties of $(Ti_{0.8}Co_{0.2}O_2/Ca_2Nb_3O_{10})$ superlattices with controlled interlayer coupling. $(Ti_{0.8}Co_{0.2}O_2/Ca_2Nb_3O_{10})_4/Ti_{0.8}Co_{0.2}O_2$, an analogous structure to that of $Bi_{4-x}La_xTi_3O_{12}$, clearly exhibited ferroelectric behavior in the presence of the ferromagnetic nanosheets. The P−E curve showed a ferroelectric hysteresis behavior with a remnant polarization (P_r) of 5 μC cm^{-2} (Figure 3a), whereas the M−H curve exhibited a nearly paramagnetic nature (with a very weak ferromagnetic moment) (Figure 3b). The observed ferroelectric response is not a consequence of the leakage current; $(Ti_{0.87}O_2/Ca_2Nb_3O_{10}/Ti_{0.87}O_2)$ superlattice was highly insulating with a low leakage current of <10^{-7} A cm^{-2}. We also investigated the insulating behavior in a few perovskite layers using conducting AFM (Figure S5). $Ca_2Nb_3O_{10}$ nanosheet showed a highly insulating behavior even in the 1.5 nm thick monolayer. Although the boundaries in the monolayer LB films formed conducting paths, LB deposition of another monolayer eliminated conducting paths, thereby suppressing leakage currents in the bilayer films. These observations indicate that the ferroelectric response is an intrinsic signature from the heterointerface.

To further study the interface effects, we checked the stacking dependence of the polarization and magnetization in the $(Ti_{0.8}Co_{0.2}O_2/Ca_2Nb_3O_{10})$ superlattices with different stacking sequences (Figure 3c−h). In these superlattices, we controlled the separation between the ferromagnetic nanosheets by tuning the thicknesses of the ferromagnetic $Ti_{0.8}Co_{0.2}O_2$ and dielectric $Ca_2Nb_3O_{10}$ layers. With this approach, we can control the interfacial effects on polarization and ferromagnetic coupling. Clearly, the superlattices showed a strong impact of the heterointerfaces on the polarization response; an increased number of the $(Ti_{0.8}Co_{0.2}O_2/Ca_2Nb_3O_{10})$ heterointerfaces enhanced the polarization value with a stronger ferroelectricity. We note rather complex behaviors in the magnetization. An increase in the thickness of the ferromagnetic $Ti_{0.8}Co_{0.2}O_2$ layers enhanced the magnetization. However, an enlarged separation between the ferromagnetic layers strongly reduced the magnetization; the magnetization was almost suppressed at a separation distance of grater than 3 nm. The best balance for the multiferroic behavior was obtained in $[(Ti_{0.8}Co_{0.2}O_2)_2/Ca_2Nb_3O_{10}]_2/(Ti_{0.8}Co_{0.2}O_2)_2$, in which weak ferroelectricity coexisted with ferromagnetism. The RT ferromagnetic behavior was also evidenced from a well-saturated M−H loop with a magnetic moment of ∼1 emu cm^{-3}.

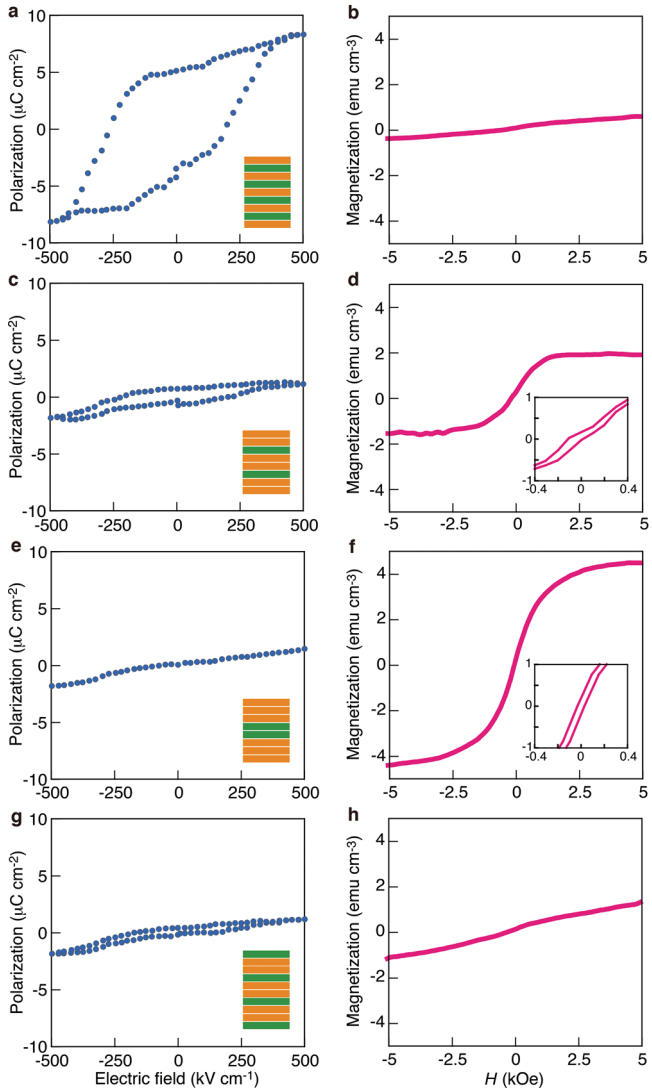

Figure 3. Polarization (P−E) and magnetization (M−H) properties for artificial superlattices with tuning interlayer coupling. (a and b) $(Ti_{0.8}Co_{0.2}O_2/Ca_2Nb_3O_{10})_4/Ti_{0.8}Co_{0.2}O_2$; (c and d) $[(Ti_{0.8}Co_{0.2}O_2)_2/Ca_2Nb_3O_{10}]_2/(Ti_{0.8}Co_{0.2}O_2)_2$; (e and f) $(Ti_{0.8}Co_{0.2}O_2)_3/(Ca_2Nb_3O_{10})_2/(Ti_{0.8}Co_{0.2}O_2)_3$; and (g and h) $Ca_2Nb_3O_{10}/[(Ti_{0.8}Co_{0.2}O_2)_2/Ca_2Nb_3O_{10}]_3$. The enlarged M−H curves are shown in d and f. The P−E and M−H measurements were performed on $SrRuO_3$ and glass substrates, respectively. All measurements were recorded at 300 K. The electric and magnetic fields are normal to the film surface.

In $[(Ti_{0.8}Co_{0.2}O_2)_2/Ca_2Nb_3O_{10}]_2/(Ti_{0.8}Co_{0.2}O_2)_2$ superlattice, the coexistence of ferromagnetism and ferroelectricity also induced an ME coupling (Figure 4). The dielectric/

DOI: 10.1021/jacs.6b02722
J. Am. Chem. Soc. 2016, 138, 7621−7625

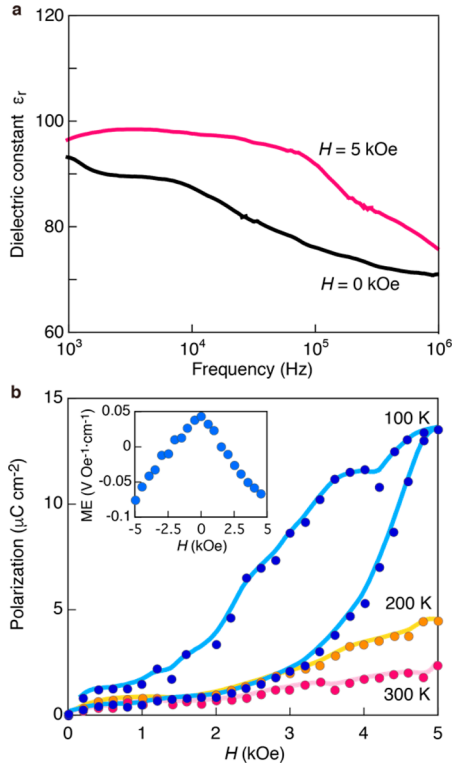

Figure 4. Magnetoelectric effect of an artificial superlattice. (a) Frequency dependence of dielectric constant (ε_r) for $[(Ti_{0.8}Co_{0.2}O_2)_2/Ca_2Nb_3O_{10}]_2/(Ti_{0.8}Co_{0.2}O_2)_2$ on a $SrRuO_3$ substrate under a magnetic field. The magnetic field is normal to the film surface. The measurements were recorded at 300 K. (b) Magnetic-field control of electric polarization (P_r) of the same film sample measured at 100, 200, and 300 K. The magnetic field is normal to the film surface.

ferroelectric responses showed a strong dependence on the magnetic field even at RT. The dielectric response (ε_r) exhibited strong frequency dependence in the regime of 10 kHz to 1 MHz, in contrast to the flat dispersion observed in the $(Ca_2Nb_3O_{10})_{10}$.[11] In $[(Ti_{0.8}Co_{0.2}O_2)_2/Ca_2Nb_3O_{10}]_2/(Ti_{0.8}Co_{0.2}O_2)_2$ superlattice, the ε_r value remained stable between 10^3 and 10^4 Hz, but gradually decreased at higher frequencies (Figure 4a). The plateau region showing a stable dielectric response was gradually expanded up to $\sim 10^5$ Hz at 5 kOe. We also observed a clear magneto-capacitance effect; a substantial increase in ε_r was achieved at a higher magnetic field. The maximum value of the magneto-capacitance, as defined by $\varepsilon(H)/\varepsilon(0)$, reached ~10% at 5 kOe. We also note a similar enhancement of the magneto-capacitance in $Ca_2Nb_3O_{10}/[(Ti_{0.8}Co_{0.2}O_2)_2/Ca_2Nb_3O_{10}]_3$ (Figure S6). Furthermore, this superlattice enabled the magnetic field control of the polarization state (Figure 4b); the electric polarization (P) was increased under the applied magnetic field. This is a clear signature of a strong ME coupling between polarization and magnetization, which is more pronounced at 100 K. We also checked the ME coefficient at RT by the means of the magnetic-field-induced electric voltage technique (inset of Figure 4b). The observed ME coefficient was ~0.1 V $Oe^{-1}\cdot cm^{-1}$ at $H = 0$, which is comparable with those for Aurivillius compounds with ME effects.[18] These results provide direct evidence of the possibility of magnetic field control of the electrical polarization in the nanosheet superlattices.

We now consider the microscopic mechanisms of ME coupling in the nanosheet superlattices. In general, multiferroic can be categorized into two types, based on whether the ferroelectric and magnetic orders are uncorrelated or derived from one another.[6,19] In Type-I multiferroics, ferroelectricity and magnetism arise from different chemical species with ordering temperatures largely independent of one another and weak ME coupling. The ferroelectric ordering also typically appears at temperatures higher than the magnetic ordering temperature, and the spontaneous polarization P_s is large (>30 $\mu C\ cm^{-2}$) because it is driven by a second-order Jahn−Teller distortion, e.g., $BiFeO_3$. In Type-II multiferroics, however, the magnetic order induces ferroelectricity, which indicates a strong ME coupling. Nonetheless, P_s is usually much smaller (<0.1 $\mu C\ cm^{-2}$) than in Type-I cases. In a few multiferroics with high T_C (i.e., $BiFeO_3$ and $Sr_{1-x}Ba_xMnO_3$), magnetism is caused by Mott physics arising from strong correlations; the interactions localize the spins at high temperatures, paving the way for magnetic ordering at RT.[20−22] Materials in which this robust magnetism is coupled with ferroelectric distortions are ideal candidates for RT multiferroics.

Our nanosheet superlattices are a unique type of RT multiferroics in which layered perovskite architectures adopt unusual polar tilts and rotations of the NbO_6 octahedra, providing a new route to interface-induced ferroelectricity coupled with ferromagnetic modules. This situation has a close resemblance to our previous studies of artificial ferroelectrics. In $(LaNb_2O_7/Ca_2Nb_3O_{10})$ and $(Ti_{0.87}O_2)$ $(Ca_2Nb_3O_{10})_2$-$(Ti_{0.87}O_2)$ superlattices, the heterointerfaces with a broken symmetry produce a new environment of interlayer coupling, giving rise to ferroelectricity.[14,23] We expect similar ferroelectric instability even in cases of coupling with ferromagnetic nanosheets; the adjoined nanosheets possess a weak bonding with highly polar NH_4^+ ions, which facilitates a zone-boundary ferroelectric distortion coupled with the distortion of the NbO_6 octahedra at the interface (Figure 1e). We thus conclude that the ferroelectric property originates from the asymmetrical environments at the interfaces, and the soft interfaces with highly polar NH_4^+ ions cause a strong coupling between the ferroelectric displacement and antiferrodistortive motion of the NbO_6 octahedra, similar to the ferroelectric/antiferrodistortive coupling in observed in ferroelectric/paraelectric superlattices with improper ferroelectricity.[24]

However, the multiferroic behaviors are somewhat surprising. We expect that the superlattices do not affect the electronic structures because of the electronically isolated nature of the self-assembled structures. To investigate the electronic structure of the superlattice films, we performed hard X-ray photoemission spectroscopy (Figure S6). A comparison of the spectral line shapes and the peak positions for Ti 2p, Co 2p, and Nb 3d peaks revealed that the oxidation states of Co and Nb ions in $(Ti_{0.8}Co_{0.2}O_2/Ca_2Nb_3O_{10})_4/Ti_{0.8}Co_{0.2}O_2$ superlattice remained unchanged from those of the same ions in the multilayer films of $(Ca_2Nb_3O_{10})_{10}$ and $(Ti_{0.8}Co_{0.2}O_2)_{10}$, implying the absence of charge transfer at $(Ti_{0.8}Co_{0.2}O_2/Ca_2Nb_3O_{10})$ heterointerfaces. These results indicate that the ME behaviors comes from a strong magnetic coupling across the neighboring nanosheets. In ferromagnetic $Ti_{0.8}Co_{0.2}O_2$ nanosheets, surface Co spins and their spin−orbit couplings are very strong because of the entire surface nature of 2D nanosheets.[25,26] This type of spin−orbit interaction strongly affects the magnetic properties of the nanosheet superlattices, which tends to result in the cross-coupling of spins and electric dipoles at $(Ti_{0.8}Co_{0.2}O_2/Ca_2Nb_3O_{10})$ heterointerfaces in the superlattices. In the nanosheet superlattices, $(Ti_{0.8}Co_{0.2}O_2/$

DOI: 10.1021/jacs.6b02722
J. Am. Chem. Soc. 2016, 138, 7621−7625

$Ca_2Nb_3O_{10}$) heterointerfaces exploited the reduction in symmetry associated with an interface to permit polarization and ME response where it would otherwise be symmetry-prohibited. Ferroelectric distortions are driven by a combination of steric and electrostatic effects that are compatible with the presence of ferromagnetic $Ti_{0.8}Co_{0.2}O_2$ layers. A technologically relevant problem that has received recent interests is ferroelectrically induced weak ferromagnetism in a single-phase multiferroic material.[24] Recent first-principles calculations have predicted new multiferroics, in which weak ferromagnetism is coupled with a polar lattice distortion.

■ CONCLUSIONS

Our observations unambiguously confirm the coexistence of ferromagnetism and ferroelectricity, as demonstrated by artificial superlattices composed of ferromagnetic $Ti_{0.8}Co_{0.2}O_2$ and dielectric $Ca_2Nb_3O_{10}$ nanosheets. Such an artificial structuring allows us to engineer the interlayer coupling, and ($Ti_{0.8}Co_{0.2}O_2/Ca_2Nb_3O_{10}/Ti_{0.8}Co_{0.2}O_2$) superlattices induce room-temperature ferroelectricity in the presence of the ferromagnetic order. Furthermore, exquisite control of the ME effects can be achieved by tuning the interlayer coupling (i.e., the stacking sequence) and/or the composition of nanosheets (i.e., controlled doping). In ferromagnetic $Ti_{1-x-y}Fe_xCo_yO_2$ and dielectric $Ca_{2-x}Sr_xNb_{3-y}Sr_yO_{10}$ nanosheets,[9,27] we can tune the electronic properties, offering another option for tailored ME properties by doping.

In the multiferroic field, the current target is designing materials with a strong magnetoelectric coupling. In this work, we have demonstrated a rational design for artificial multiferroics using 2D nanosheets. Considering the versatility of materials choice and their coupling intensity at the nanosheet interfaces, we can create a new kind of layered perovskite multiferroics with a tailored ME coupling. Our approach opens up new opportunities to understand ferroic coupling and enables heretofore unachievable engineering of ferroic and electronic functionalities.

■ ASSOCIATED CONTENT

Supporting Information

The Supporting Information is available free of charge on the ACS Publications website at DOI: 10.1021/jacs.6b02722.

Experimental details; AFM images; UV−vis spectra; in-plane XRD data; *P*−*E* property data; magnetic modulation data; Ti 2p, Co 2p, and Nb 3d core level HX-PES spectra (PDF)

■ AUTHOR INFORMATION

Corresponding Authors

*E-mail: osada.minoru@nims.go.jp.

*E-mail: sasaki.takayoshi@nims.go.jp.

Notes

The authors declare no competing financial interest.

■ ACKNOWLEDGMENTS

This work was supported in part by the World Premier International Research Center Initiative on Materials Nanoarchitronics (WPI-MANA), MEXT, CREST, JST, and Grant-in-Aid for Scientific research, JSPS, Japan. The HX-PES measurements were performed under the approvals of NIMS Synchrotron X-ray Station (Proposal Nos. 2010A4608, 2012B4608, 2013A4603, 2015B4605). The authors are grateful to HiSOR, Hiroshima University and JAEA/SPring-8 for the development of HX-PES at BL15XU of SPring-8.

■ REFERENCES

(1) Spaldin, N. A.; Fiebig, M. *Science* **2005**, *309*, 391.
(2) Eerenstein, W.; Mathur, N. D.; Scott, J. F. *Nature* **2006**, *442*, 759.
(3) Ramesh, R.; Spaldin, N. A. *Nat. Mater.* **2007**, *6*, 21.
(4) Wang, Y.; Hu, J. M.; Lin, Y. H.; Nan, C.-W. *NPG Asia Mater.* **2010**, *2*, 61.
(5) Fernandes Vaz, C. A.; Staub, U. *J. Mater. Chem. C* **2013**, *1*, 6731.
(6) Hill, N. A. *J. Phys. Chem. B* **2000**, *104*, 6694.
(7) Schlom, D. G.; Chen, L. Q.; Pan, X. Q.; Schmehl, A.; Zurbuchen, M. A. *J. Am. Ceram. Soc.* **2008**, *91*, 2429.
(8) Osada, M.; Ebina, Y.; Fukuda, K.; Ono, K.; Takada, K.; Yamaura, K.; Takayama-Muromachi, E.; Sasaki, T. *Phys. Rev. B: Condens. Matter Mater. Phys.* **2006**, *73*, 153301.
(9) Osada, M.; Yoguchi, S.; Itose, M.; Li, B.-W.; Ebina, Y.; Fukuda, K.; Kotani, Y.; Ono, K.; Ueda, S.; Sasaki, T. *Nanoscale* **2014**, *6*, 14227.
(10) Ebina, Y.; Sasaki, T.; Watanabe, M. *Solid State Ionics* **2002**, *151*, 177.
(11) Osada, M.; Akatsuka, K.; Ebina, Y.; Funakubo, H.; Ono, K.; Takada, K.; Sasaki, T. *ACS Nano* **2010**, *4*, 5225.
(12) Muramatsu, M.; Akatsuka, K.; Ebina, Y.; Wang, K.; Sasaki, T.; Ishida, T.; Miyake, K.; Haga, M. *Langmuir* **2005**, *21*, 6590.
(13) Akatsuka, K.; Haga, M.; Ebina, Y.; Osada, M.; Fukuda, K.; Sasaki, T. *ACS Nano* **2009**, *3*, 1097.
(14) Li, B. W.; Osada, M.; Ozawa, T. C.; Ebina, Y.; Akatsuka, K.; Ma, R.; Funakubo, H.; Sasaki, T. *ACS Nano* **2010**, *4*, 6673.
(15) Sasaki, T.; Ebina, Y.; Fukuda, K.; Tanaka, T.; Harada, M.; Watanabe, M. *Chem. Mater.* **2002**, *14*, 3524.
(16) Park, B. H.; Kang, B. S.; Bu, S. D.; Noh, T. W.; Lee, J.; Jo, W. *Nature* **1999**, *401*, 682.
(17) Keeney, L.; Maity, T.; Schmidt, M.; Amann, A.; Deepak, N.; Petkov, N.; Roy, S.; Pemble, M. E.; Whatmore, R. W. *J. Am. Ceram. Soc.* **2013**, *96*, 2339.
(18) Zhao, H. Y.; Kimura, H.; Cheng, Z.; Osada, M.; Wang, J.; Wang, X.; Dou, S.; Liu, Y.; Yu, J.; Matsumoto, T.; Tohei, T.; Shibata, N.; Ikuhara, Y. *Sci. Rep.* **2014**, *4*, 5255.
(19) Cheong, S. W.; Mostovoy, M. *Nat. Mater.* **2007**, *6*, 13.
(20) Wang, J.; Neaton, J. B.; Zheng, H.; Nagarajan, V.; Ogale, S. B.; Liu, B.; Viehland, D.; Vaithyanathan, V.; Schlom, D. G.; Waghmare, U. V.; Spaldin, N. A.; Rabe, K. M.; Wuttig, M.; Ramesh, R. *Science* **2003**, *299*, 1719.
(21) Kimura, T.; Goto, T.; Shintani, H.; Ishizaka, K.; Arima, T.; Tokura, Y. *Nature* **2003**, *426*, 55.
(22) Goto, T.; Kimura, T.; Lawes, G.; Ramirez, A. P.; Tokura, Y. *Phys. Rev. Lett.* **2004**, *92*, 257201.
(23) Kim, Y. H.; Dong, L.; Osada, M.; Li, B. W.; Ebina, Y.; Sasaki, T. *Nanotechnology* **2015**, *26*, 244001.
(24) Bousquet, E.; Dawber, M.; Stucki, N.; Lichtensteiger, C.; Hermet, P.; Gariglio, S.; Triscone, J.-M.; Ghosez, P. *Nature* **2008**, *452*, 732.
(25) Osada, M.; Ebina, Y.; Takada, K.; Sasaki, T. *Adv. Mater.* **2006**, *18*, 295.
(26) Fennie, C. J. *Phys. Rev. Lett.* **2008**, *100*, 167203.
(27) Osada, M.; Sasaki, T. *Adv. Mater.* **2012**, *24*, 210.

DOI: 10.1021/jacs.6b02722
J. Am. Chem. Soc. 2016, 138, 7621−7625